

Development and Corrosion Characterization of Ultra-High-Strength Steels

A. Torres-Islas^{1,*}, FV Guerra², A Bedolla-Jacuinde², A. Molina-Ocampo³, S. Serna³,
B. Campillo⁴, and H. Martinez⁵

¹ Facultad de Ciencias Químicas e Ingeniería P.A. Ing. Mecánica, Universidad Autónoma del Estado de Morelos, Av. Universidad 1001, Col. Chamilpa, C.P. 62209, Cuernavaca, Morelos, México.

² Instituto de Investigación en Metalurgia y Materiales, Universidad Michoacana de San Nicolas de Hidalgo Gral. Francisco J. Mugica S/N Felicitas del Rio Morelia Michoacan - 58030, México.

³ Centro de Investigación en Ingeniería y Ciencias Aplicadas, Universidad Autónoma del Estado de Morelos, Av. Universidad 1001, Col. Chamilpa, C.P. 62209, Cuernavaca, Morelos, México.

⁴ UNAM, Facultad de Química/Instituto de Ciencias Físicas, Coyoacan, 04510 México, DF, México

⁵ Laboratorio de Espectroscopia, Instituto de Ciencias Físicas, Universidad Nacional Autónoma de México, A.P. 48-3, C.P. &2210, Cuernavaca - 62210, Morelos México.

*E-mail: alvaro.torres@uaem.mx

Received: 14 July 2020 / Accepted: 22 August 2020 / Published: 30 September 2020

Potentiodynamic polarization and electrochemical impedance spectroscopy measurements were used to investigate the corrosion behavior and mechanical properties of three different quenched and quenched/tempered ultra-high-strength steel alloys in contact with alkaline and acid aqueous solutions. The results are analyzed on the basis of the corrosion potential E_{corr} and the corrosion current density I_{corr} . Continuous anodic dissolution is the main type of corrosion driven by a charge-transfer mechanism in all of the investigated steel conditions irrespective of the phases present. The observed solubilities of iron and its oxides and hydroxides respectively agreed with the reactions $\text{Fe}_2\text{O}_3 + \text{H}_2\text{O} \rightarrow \text{Fe}(\text{OH})_2^+$ and $2\text{Fe}^{3+} + 3\text{H}_2\text{O} \rightarrow \text{Fe}_2\text{O}_3 + 6\text{H}^+$. In addition, the Mo and V content played important roles in determining the corrosion levels, as did redox reactions and microconstituents present in the various steel phases. The quenched/tempered steel exhibited the best corrosion and mechanical properties.

Keywords: UHSS alloys, Corrosion resistance, Mo and V additions, Alkaline and acid solutions, Mechanical properties.

1. INTRODUCTION

At present, the automotive industry is focused on processing advanced steels with a high strength-to-ductility ratio and low weight compared with those of conventional high-strength steels.

Advanced high-strength steels are a new class of materials developed to maintain high strength while also exhibiting the high formability characteristics required for processing, thus incurring reasonably low production costs. The first and second generations of advanced high-strength steels showed some limitations: the first generation had high strength but low formability, whereas the second generation had good strength and ductility but incurred high production costs. Among the various advanced high-strength steels (e.g., dual-phase steels, steels with an induced phase transformation, and complex-phase steels), all are considered good options as the basis for development of the third generation of advanced high-strength steels, currently known as ultra-high-strength steels (UHSSs).

UHSSs are expected to offer excellent performance and ductility with a good combination of weldability, formability, and toughness. They are also expected to offer a wide range of applications in the manufacture of, e.g., pipes, automobiles, pressure vessels, ships, offshore platforms, aircraft, trains, and rocket engine housings. In particular, steel with a tensile strength greater than 1400 MPa is suitable for cold working of structural and automotive components. To ensure good safety characteristics, microalloying elements such as Ti, Ni, and V, combined with small amounts of C, are expected to impart such steels with good mechanical properties [1,2]. In subsequent heat treatments, these microalloying elements precipitate as carbides and/or carbonitrides at textures sufficiently fine to prevent the movement of dislocations; this lack of dislocation movement results in a substantial increase in steel strength [3]. In practical design, however, other factors must be considered for adequate performance, including rigidity, corrosion resistance, shock resistance, and fatigue [4].

The main research topic in our previous works [5–11] has been the mechanical properties of UHSSs. However, as previously mentioned, other factors influence performance in various practical applications; among these factors, corrosion resistance is critical. The aim of the present study was to develop three different alloys, taking as references the compositions of steels studied in recent years. In this analysis, alloys with various elemental compositions were characterized electrochemically to determine their corrosion resistance.

2. EXPERIMENTAL PROCEDURE

2.1 *Manufacture and heat treatment of ultra-high-strength steel alloys*

High-purity elements used to manufacture the UHSS alloys were melted in a high-vacuum induction furnace. Three different alloys, denoted as L1, L2, and L3, were prepared by varying mainly the Mo and V contents. The elemental analysis of each steel was carried out using the spark spectrometry technique with a Bruker Q8 Magellan sparc emission spectrometer.

To determine how the microstructure of each steel influenced its corrosion behavior, each steel was subjected to two heat treatments: quenching and quenching/tempering. Before the heat treatments, each steel was cut into $1 \times 1 \times 1 \text{ cm}^3$ specimens that were subsequently sanded with 600 grit sandpaper and cleaned with acetone. In the quenching treatment, the steel was heated to 850 °C for 40 min and cooled in oil at room temperature; for the tempering treatment, the tempered steel was heated to 350 °C for 30 min and then left to cool in the furnace.

Rockwell C hardness tests were also performed on the steels prepared under each of the aforementioned conditions. With the hardness data, the ultimate tensile strength (UTS) of each steel was calculated and compared with the results from simulations conducted using the JMatPro software. The phases present in the steel were determined on the basis of a comparison with the simulation results [12–16].

2.2 Sample preparation and corrosion testing

The specimens for the corrosion tests were prepared by cutting each steel into $1 \times 1 \times 1 \text{ cm}^3$ cubes per side, welding a nichrome wire onto each specimen, and encapsulating the welded pair with epoxy resin. Before and after each test, the surface was sanded with 600 grit sandpaper. The test solutions were prepared using distilled water and analytical-grade reagents H_2SO_4 and NaCl . Prior to each test, the pH values of the test solutions were adjusted to 3, 5, 9, or 11. The pH measurements were conducted with an Oakton digital pH meter that had been previously calibrated. The amount of aqueous solution used in each test was 100 mL. To ensure the reproducibility of the results, triplicate experimental measurement were carried out and the solution was changed after each test. To monitor corrosion behavior, an automated potentiostat (Applied Corrosion Monitoring, Ltd.) connected to a personal computer was used and electrochemical potentiodynamic polarization techniques were employed. Polarization from -100 to 1500 mV was applied with a scan rate of 60 mV/min . Electrochemical impedance spectroscopy (EIS) tests were performed in the frequency range from 0.01 Hz to 10 kHz . Each test was conducted in triplicate. The results were analyzed in terms of the following parameters: corrosion potential (E_{corr}), corrosion current density (I_{corr}), impedance modulus (Z), and phase angle. The I_{corr} was calculated via the Tafel extrapolation method using the anode branch. In the electrochemical cell arrangement, the steel specimen was the working electrode, an Ag/AgCl electrode was the reference electrode, and a graphite electrode was the counter electrode. All tests were conducted at room temperature.

3. RESULTS AND DISCUSSION

Table 1 shows the compositions and mechanical properties of the studied steels denominated as L1, L2, and L3, as well as those of UHSS steels reported in the literature. Table 1 also shows the compositions of the studied steels. The C, Mn, Si, Ni, and Cr contents were constant; only the Mo and V contents were varied. This limit on variation was imposed to clearly evaluate the effects of these elements on the mechanical and corrosion properties of the steel. All other elements present were considered impurities.

Table 1. Composition and mechanical properties of ultra-high-strength steels reported in the literature and those investigated in the present study.

Reference	C	Mn	Si	Ni	Cr	Al	Ti	Nb	S	P	N	Mo	V	Cu	B	Fe	UTS (Mpa)
1	0.79	0.34	0.8		0.9								0.06			Bal	1715
5	0.28	1.76	0.35	4.4		0.02	0.06	0.08	0.01	0.01	0.0068	1.88				Bal	1991
6	1.43	0.7	0.55	1.39	2.19			0.02				0.76	0.08			Bal	
7	0.79	0.34	0.8		0.9								0.06			Bal	1715
8	0.06	1.31	0.6	6.09	17.16									2.08		Bal	737
9	0.18	2.45	1.03	0.3	0.02	0.01			0.009	0.003						Bal	1265
10	0.095	1.47	0.21	0.32	0.45	0.0236	0.015		0.0012	0.009		0.46	0.033	0.31	0.018	Bal	799
11	0.2	2	1	0.6	0.8							0.2				Bal	1402
Alloy L1	0.4	0.8	0.72	0.0071	0.95	0.03	0.0043	0.02	0.011	0.018		2	0.086	0.021		bal	1465
Alloy L2	0.4	0.7	0.74	0.0064	0.86	0.03	0.0037	0.02	0.011	0.018		2.44	0.101	0.022		bal	1510
Alloy L3	0.4	0.7	0.73	0.0072	0.89	0.025	0.0035	0.02	0.012	0.017		2.84	0.11	0.026		bal	1415

Table 2 shows the hardness and UTS results for each steel in its initial, quenched, and quenched/tempered conditions.

Table 2. Hardness and ultimate tensile strength (UTS) of steel under all considered conditions.

	Hardness (HRc) / UTS (MPa)		
	L1	L2	L3
As-Received (Ar)	44/1465	45/1510	42/1415
Oil-quenched (Oq)	45/1510	47/1618	43/1465
Quenched and tempered (Qt)	42/1415	44/1465	41/1369

As shown in Table 2, the highest UTS was exhibited by the L2 Oq steel, with a value of 1618 MPa, whereas the lowest UTS was exhibited by the L3 Qt steel. In general, the L2 steel exhibited the highest UTS values under all of the investigated steel conditions. However, the phases present in each condition determined the steels' corrosion behavior, as discussed in the next paragraph.

Figure 1 shows the results of electrochemical tests for the L1 steel in all conditions, in contact with the solutions with various pH values, as represented by polarization curves and Nyquist diagrams. The results in this figure show that, in all conditions, the L1 steel showed continuous anodic dissolution behavior in solutions with pH values of 3, 5, 7, and 9. A tendency to passivate near -500 mV was observed only in the case of the pH 11 solution. However, after anodic dissolution, the E_{corr} values for the steel specimens in the different solutions were -573 mV for pH 3, -621 mV for pH 5, -466 mV for pH 7, -738 mV for pH 9, and -716 mV for pH 11. The tests at pH 7 were performed in distilled water, and the results were used as reference data. Because of the absence of ions in the pH 7 solution, the results of the EIS tests at this pH did not show a consistent behavior in the Nyquist diagrams; as evident in the polarization curves, the I_{corr} at pH 7 exhibited the lowest values because of the high resistance of the solution. By contrast, the other Nyquist diagrams in Figure 1 show semicircular curves for steels in acidic solutions, indicating that the main mechanism of steel corrosion was charge transference [17]. Despite this overall similarity in character, the modulus of the

impedance varied strongly with pH, exhibiting values of $250 \text{ } \Omega/\text{cm}^2$ for pH 3 but $1600\text{--}2000 \text{ } \Omega/\text{cm}^2$ for pH 5. These two solutions also showed the highest resistance values, differing from those of alkaline solutions by 1 and 2 orders of magnitude, respectively. On the basis of the Pourbaix diagram for Fe [18] with E_{corr} for the solutions with pH 3 and 5, the solubility of Fe and its oxides and hydroxides proceeded according to Reaction 1 in the domains of relative predominance of dissolved ions Fe_2^+ , HFeO_2^- , Fe_3^+ , $\text{Fe}(\text{OH})_2^+$, and FeO^{4-} .

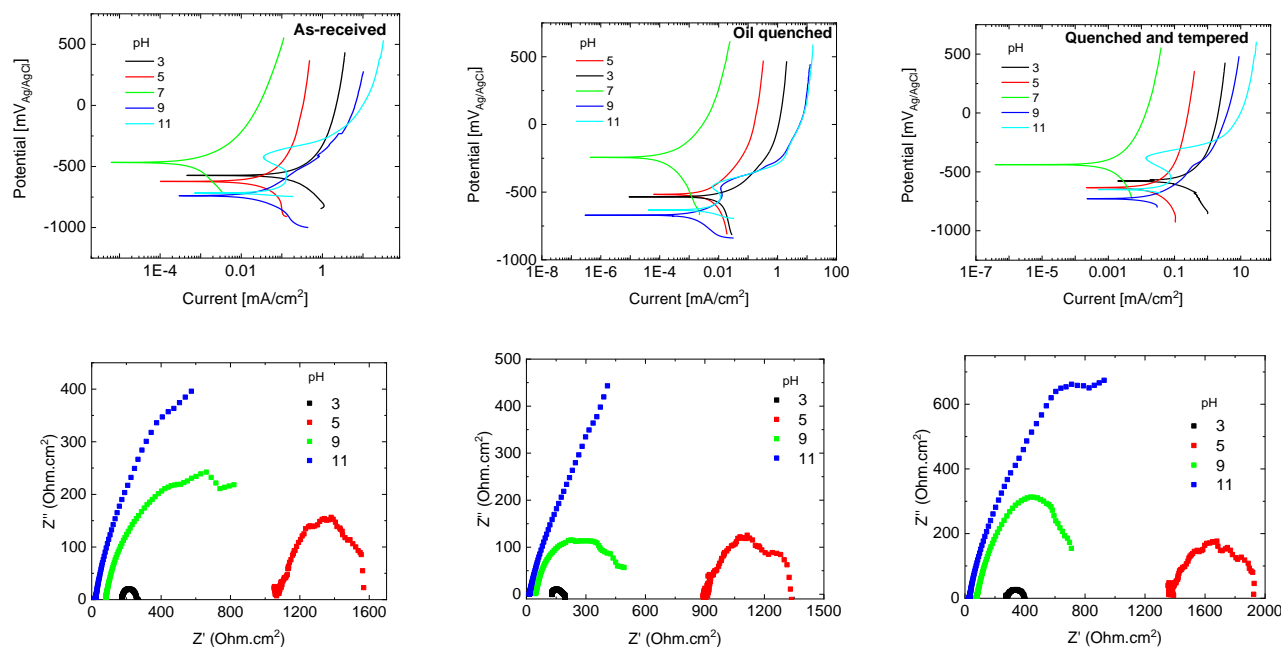
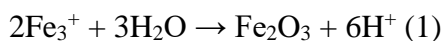


Figure 1. Polarization curves and Nyquist diagrams for alloy L1 in the as-received, oil-quenched, and quenched-and-tempered conditions, as recorded with the alloy in acidic and alkaline solutions.

In this reaction, Fe_2O_3 is assumed to be a passive oxide that persists only in the absence of substances that can form soluble complexes or insoluble salts with Fe [18]. In such circumstances, the presence of H_2SO_4 most likely indicates the presence of this type of salt, which prevents ionization of the solution, thereby increasing its resistance. At the same time, it prevents the steel from being passive, as evident in the polarization curves for the L1 steel in all conditions. This mechanism can also lower the capacitance, as suggested by the semicircular polarization curves corresponding to acidic solutions (Figure 1).

The aforementioned idea is supported by the phase-angle behavior for the steel in acidic solutions in the Bode plots in Figure 2. This figure shows that, for the L1 steel in pH 3 and 5 solutions, the phase angle at low frequencies was approximately 5° , indicating that the layer of corrosion products on the surface of the steel was quite permeable and not protective. However, in alkaline solutions, the phase angle at low frequencies is approximately 30° and 50° for steel specimens in solutions of pH 9 and 11, respectively. In the Nyquist diagrams in Figure 1, the polarization curve for

the steel specimen in the pH 9 solution tends to form a semicircle, indicating the existence of a charge-transfer mechanism. By contrast, the curve for the specimen in the pH 11 solution tends to be rectilinear at an angle of 45°. This behavior is related to the mechanism of continuous dissolution, casting doubt on the existence of a passive state despite the aforementioned phase-angle behavior and Nyquist diagrams. However, the corrosion products that formed on the surface of the steel in these solutions increased the capacitance and conductivity of the solution, as observed in the phase angle and Z' values in the Nyquist diagrams, where Z' represents the real component of impedance. This finding means that the Na^+ and Cl^- ions dissociated in the H_2O , facilitating the formation of $\text{Fe}(\text{OH})_2^+$ according to Reaction 2 as shown in the Pourbaix diagram for Fe.

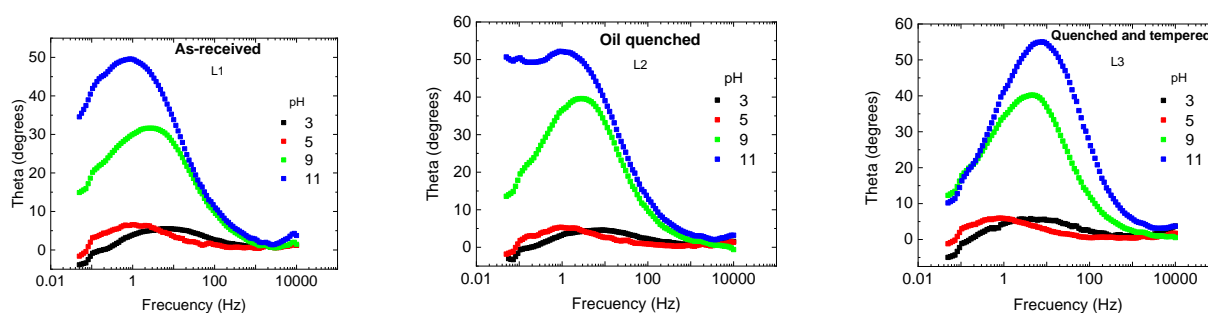
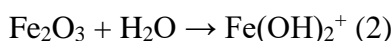


Figure 2. Phase-angle diagrams for alloys L1 as-received, L2 oil-quenched, and L3 quenched-and-tempered in acidic and alkaline solutions.

At the corresponding pH and potential values in the Pourbaix diagram, the formation of $\text{Fe}(\text{OH})_2^+$ led to passivation; however, because of effects along the border between the zones of passivation and corrosion, the L1 steel under all conditions could not be passivated. El-Mahdy. [19] have suggested that the variation in E_{corr} for this type of steel in contact with NaCl solution is attributable to competition between the processes of formation and dissolution of the passivation layer, as evident in the polarization curves in Figure 1. The most noble E_{corr} values were exhibited by steels in alkaline solutions, mainly because the redox reactions reached equilibrium faster than in acidic solutions.

Nyquist and phase-angle diagrams reveal that the polarization-curve behaviors of the L2 steels are similar to those of the L3 steels. Figures 4 and 5 show the polarization curves for the L2 and L3 steels, respectively. The Nyquist diagrams are not presented because they are identical to that of the L1 steel; Figure 2 shows only the phase-angle Bode plots for the L2 Oq and L3 Qt steels.

In general, the aforementioned behavior corresponds electrochemically to the processes of polarization by concentration and activation, respectively. As observed in solutions with acidic pH, the electrochemical reactions are controlled by the diffusion of ions in the electrolyte such that the H^+ ions diffuse to the surface of the metal, forming H_2 gas via the cathodic reaction $2\text{H}^+ + 2\text{e}^- \rightarrow \text{H}_2$, giving rise to reaction (1). Therefore, the changes in the dissolved substances increase the diffusion rate of the ions, decreasing the effects of polarization by concentration, thereby increasing the corrosion rate and

the E_{corr} . By contrast, in solutions with alkaline pH, a mechanism of polarization by activation occurs, where the activation energy most likely reduces the cathodic H_2 in a slower stage than in concentration polarization, causing the anodic reaction $2OH^- \rightarrow \frac{1}{2}O_2 + H_2O + 2e^-$, leading to reaction (2). This behavior has also been observed in other systems [20-23].

The parameters of the EIS tests simulated in the Zview software for the steel in contact with the different solutions are shown in Table 3. When analyzing the data, we observed that the resistance of the solution (R_s) is lower in the solutions with pH 9 and 11, respectively, which is consistent with the Nyquist diagrams. In the same table, the values of the double layer constant-phase element (CPEdl) are presented; the solutions with pH 3 and 5 show the lowest values, which means that the capacitance of the double layer as a function of the impedance modulus $|Z|$ should exhibit a relatively high charge-transfer gradient. However, the values of the charge-transfer resistance R_{ct} in Table 3 show the opposite behavior, indicating the existence of a concentration polarization mechanism in which, as previously mentioned, changes in the dissolved substances (i.e., rust or corrosion products) increase the rate of diffusion of ions. This effect is related to the presence of an oxide layer on the surface of the steel that is not very protective and is quite permeable. This interpretation is supported by the phase-angle behavior in the Bode diagrams and the simulated values in Table 3 of the oxide constant-phase element (CPEox) for acid solutions. However, the values of the simulated parameters for the alkaline solutions are in accordance with Reaction 2 because of the composition of the hydroxide, the values of the oxide constant-phase element (CPEox), in particular, and the phase-angle behavior in the Bode diagrams. Representative electrical elements and parameters conform to the equivalent circuit in Figure 3.

Table 3. EIS simulation parameters for alloy L1 in acidic and alkaline solutions.

pH	R_s ($W.cm^2$)	CPEdl ($W^{-1}Xs^{-n}Xcm^{-2}$)	R_{ct} ($W.cm^2$)	CPEox ($W^{-1}Xs^{-n}Xcm^{-2}$)
3	62.74	5.36E-04	398.8	0.67226
5	174.2	3.26E-03	93.7	0.4446
9	11.6	1.94E-03	283.7	0.77369
11	11.6	1.94E-03	283.7	0.77369

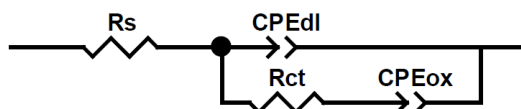


Figure 3. Equivalent circuit used to model the impedance spectra for the corrosion data of L1, L2, and L3 alloys in acidic and alkaline solutions.

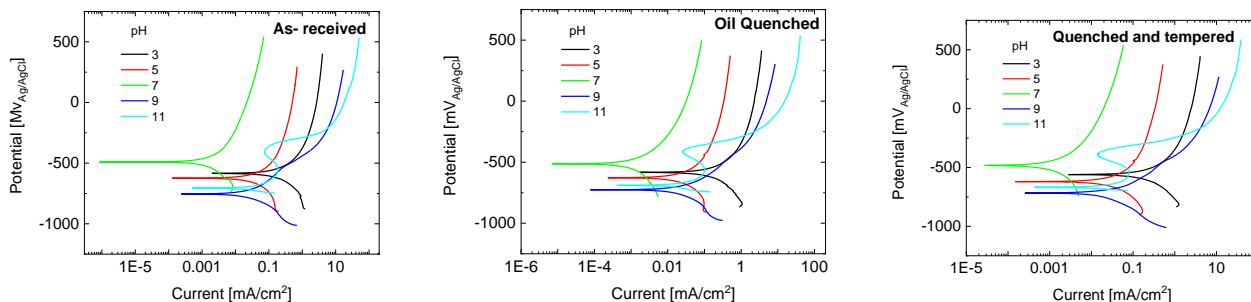


Figure 4. Polarization curves for alloy L2 in the as-received, oil-quenched, and quenched-and-tempered conditions, as recorded with the alloy in acidic and alkaline solutions.

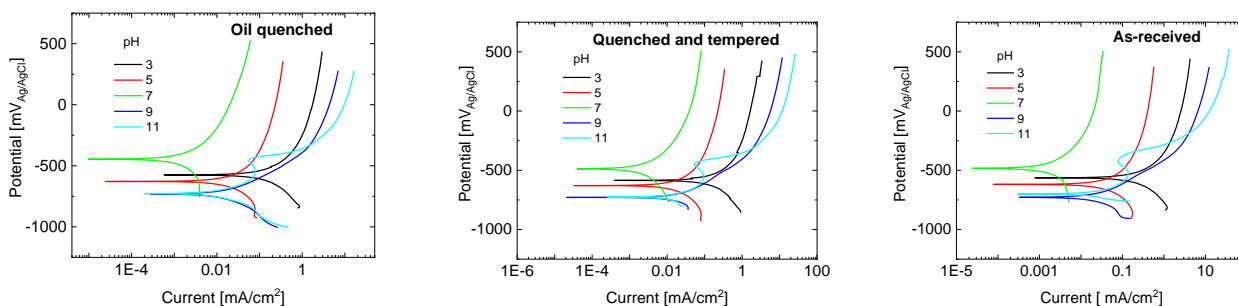


Figure 5. Polarization curves for alloy L3 in the oil-quenched, quenched-and-tempered, and as-received conditions, as recorded with the alloy in acidic and alkaline solutions.

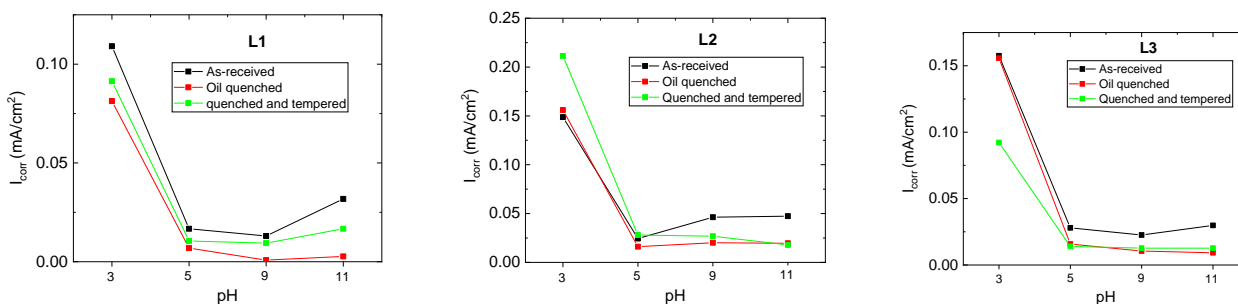


Figure 6. I_{corr} behaviors for alloys L1, L2, and L3 in the as-received, oil-quenched, and quenched-and-tempered conditions, as measured with the alloys in acidic and alkaline solutions.

The corrosion current densities I_{corr} for the L1, L2, and L3 steels in all of the considered conditions are shown in Figure 6, where the quenched/tempered L2 steel in the pH 3 solution (L2 Qt 3) exhibits the highest I_{corr} (0.2114 mA/cm^2) and L1 Oq 9 exhibits the lowest I_{corr} (0.0008 mA/cm^2). In general, for all the steels under study, the highest levels of I_{corr} were observed in the pH 3 solution, irrespective of heat treatment. The I_{corr} values were drastically lower in the pH 5 and 9 solutions; however, they increased slightly from the pH 9 solution to the pH 11 solution, in which all of the steels under all conditions exhibited the lowest levels of corrosion. However, despite the aforementioned behavioral similarities, differences were evident among the I_{corr} values of the various steels under

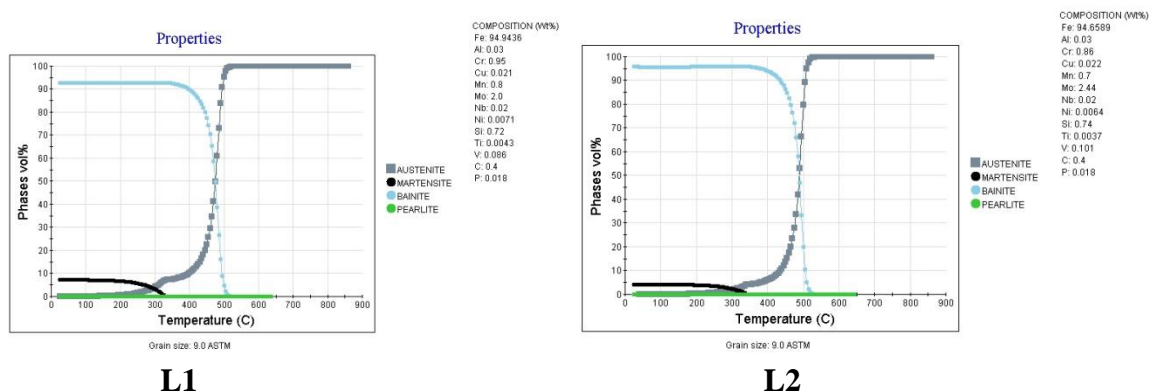
various conditions. The lowest levels of corrosion were exhibited by the L1 steel in all conditions in both acidic and alkaline solutions. The lowest I_{CORR} values were exhibited by the L1 Oq steel in solutions with pH 5, 9, and 11.

Figure 7 shows the percentage by volume of phases present for the L1, L2, and L3 steels in the Oq condition. The L1 steel exhibits highest percentage of martensite (9%), followed by the L2 steel (5%) and the L3 steel (~3%). This figure also shows that the L1 steel presents the lowest percentage of bainite. To a great extent, the corrosion behavior of Oq steel is directly related to the galvanic microparts formed in its microstructure. Martensite, as a carbon-supersaturated solid Fe phase, acts as a cathode in the presence of ferrite and bainite. However, Qt steel causes the martensite present in Oq steel to transform into tempered martensite, increasing its resistance to UTS without affecting its theoretical compositional percentage in the steel [19].

As shown in Figure 6, for all of the Qt specimens, the I_{CORR} values were elevated compared with the those of Oq specimens. This behavior can be explained by the atomic diffusion in a metastable martensite/martensite matrix during martensite tempering. This process would allow the system to evolve to the two equilibrium phases of ferrite and cementite (Fe_3C). The annealed martensite would then no longer be a phase as such; fine particles of the cementite phase in a ferritic matrix would diminish the cathodic behavior of carbon in the galvanic microparts because of its dispersal in contact with a larger quantity of ferrite acting as an anode. The Ar steels presented the highest I_{CORR} index because of the composition of the phases in the microstructure, as indicated by the analyses of the Oq and Qt steels.

Figure 6 shows that, in general, the highest and lowest levels of corrosion were exhibited by the L3 and L1 steels, respectively. The Mo and V contents clearly play important roles in corrosion behavior irrespective of the phases present. That is, for these UHSS steels, in particular, the higher the Mo and V contents, the higher the I_{CORR} . This phenomenon is mainly attributable to the precipitation of intermetallic compounds and secondary phases that affect the cathodic and anodic behavior of the main constituent phases in each condition of the steel [24].

The L2 Ar steel exhibited the highest UTS resistance (1510 MPa). After heat treatment, however, the UTS resistance of the L2 Oq steel increased to 1618 MPa. Nevertheless, hardened steel tends to be more mechanically fragile because of the residual strength of its microstructure. However, the Qt treatment conferred greater tenacity; consequently, the L2 Qt steel exhibited the highest mechanical resistance, with a UTS value of 1465 MPa.



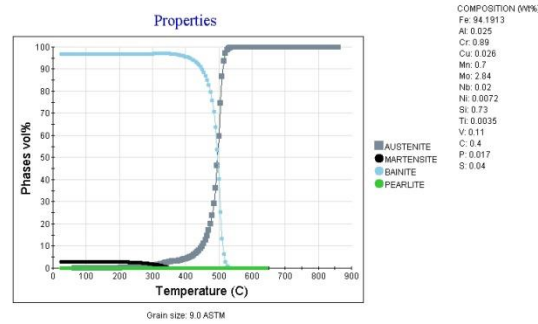


Figure 7. JMatPro simulation phases after quenching for alloys L1, L2, and L3.

Despite the aforementioned results, the L1 Qt steel still exhibited the lowest I_{corr} value; thus, in the present study, the L1 Qt exhibited the best mechanical and corrosion resistance properties. In addition, the corrosion by anodic dissolution that all steels exhibit to a certain extent is less undesirable than a pitting corrosion mechanism. This statement is especially true considering that a passive layer is a condition for the existence of a localized corrosion mechanism that could render the steel susceptible to catastrophic failure.

5. CONCLUSIONS

- 1- The UHSS steels under study, when in contact with acidic and alkaline solutions, exhibited continuous anodic dissolution driven by a mechanism of charge transference.
- 2- The E_{corr} and I_{corr} values for each of the steel conditions were directly related to the phases present in the steel and thereby to the Mo and V contents.
- 3- The redox reactions present in the corrosion mechanisms determined the behavior of the impedance modulus and phase angle.
- 4- The quenched-and-tempered L1 steel exhibited the best corrosion resistance and mechanical properties among all of the tested specimens.

ACKNOWLEDGEMENT

The present study was supported by PRODEP project as a short stay research México.

References

1. Z.J Xie, Y.P. Fang, G. Han, H. Guo, R.D.K. Misra, C.J. Shang, *Mater. Sci. Eng., A*, 618 (2014) 112.
2. Z. Liu, R.O. Olivares, Y. Lei, C.I. Garcia, G. Wang, *J. Alloys Compd.*, 679 (2016) 293.
3. S. Chatterjee, S.K. Ghosh, *Int. J. Metall. Eng.*, 2 (2013) 92.
4. J.O. Sperle, K. Olsson, *Proceedings of ISATA*, 1 (1996) 115.
5. G. Mandal, C. Roy, S.K. Ghosh, S. Chatterjee, *J. Alloys Compd.*, 705 (2017) 817.
6. X.Y. Cheng, H. Li, X.B. Cheng, *Micron*, 103 (2017) 22.
7. M. Wang, F. Zhang, Z. Yang, *Mater. Des.*, 114 (2017) 102.

8. C. Lei, X. Li, X. Deng, Z. Wang, G. Wang, *Mater. Sci. Eng., A*, 709 (2018) 72.
9. I. Hajiannia, M. Shamanian, M. Atapour, E. Ghassemali, N. Saeidi, *Trans. Indian Inst. Met.*, 71 (2018) 1363.
10. W. Hao, Z. Liu, W. Wu, X. Li, C. Du, D. Zhang, *Mater. Sci. Eng., A*, 710 (2018) 318.
11. G. Gao, Q. Xu, H. Guo, Xi. Gui, B. Zhang, B. Bai, *Mater. Sci. Eng., A*, 739 (2019) 404.
12. U. Diekmann, *Proceedings of COMAT 2012*.
13. U. Diekmann, A. Miron, A. Trasca, *Materials Science Forum*, 854 (2016) 163.
14. S. Olovsjö, P. Hammersberg, P. Avdovic, J.E. Ståhl, L. Nyborg, *Int. J. Adv. Manuf. Technol.*, 59 (2012) 55.
15. N. Saunders, Z. Guo, X. Li, A.P. Miodownik, J.-Ph. Schillé, *JOM*, 55 (2003) 60.
16. W. Yi, S. Feng, D. Xianping, Z. Lanting, S. Aidang, *Acta Metall. Sin.*, 46 (2010) 334.
17. H. Li, C. Dong, K. Xiao, X. Li, P. Zhong, *Int. J. Electrochem. Sci.*, 10 (2015) 10173.
18. M. Pourbaix, *Atlas of Electrochemical Equilibrium in Aqueous Solutions*, NACE, Houston, Tex, USA, 2nd edition 1974.
19. G.A. El-Mahdy, M.M. Hegaz, F- EL-T. Heikal, H. E. Mahmoud, A.M. Fathy, F.M. Sayed, *Int. J. Electrochem. Sci.*, 8 (2013) 2816.
20. A. Pardo, E. Otero, M. C. Merino, M. D. López, M. V. Utrilla, F. Moreno, *Corrosion*, 56 (2000) 411.
21. F. Pessu, R. Barker, A. Neville, *Corrosion*, 71 (2015) 1452.
22. L. Niu, Y. F. Cheng, *Appl. Surf. Sci.*, 253 (2007) 8626.
23. S. Wang, Shuaixing Wang, X. Yin, H. Zhang, D. Liu, N. Du, *Materials*, 12 (2019) 3175.
24. P. Paulraj, R. Garg, *Adv. Sci. Technol. Res. J.*, 9 (2015) 87.